Czech Technical University
in Prague

Faculty of Nuclear Sciences and Physical
Engineering

Department of Physics

BACHELOR THESIS

Interaction of antiprotons with nuclei

Jaroslava Hrtánková

2011

Supervisor: RNDr. Jiří Mareš, CSc.

Thesis tittle: **Interaction of antiprotons with nuclei**
Author: Jaroslava Hrtánková

Department: Department of Physics FNSPE CTU in Prague
Branch of study: Nuclear Engineering
Kind of thesis: Bachelor's Degree Project

Supervisor: RNDr. Jiří Mareš, CSc.

Abstract: The aim of the thesis is to explore the interaction of the antiproton with nuclear matter, in particular the effects of the strongly interacting antiproton on the dynamics of nucleons in the nuclear medium. This work first summarizes basic knowledge about antiparticles and properties of the antiproton. Next, the relativistic mean field (RMF) theory is briefly introduced and the RMF model for a nucleus with the antiproton is formulated. Results of the selfconsistent calculations of single-particle energies of the antiproton bound in a light nucleus ^{16}O, as well as the energies and densities of the core nucleons are presented. The dynamical approach revealed huge polarization effects inside the nucleus due to the presence of the antiproton, i.e., large compression of nuclear matter. We also noticed considerable increase of the binding energy of the system $^{16}\mathrm{O} + \bar{p}$, approximately 1000 MeV. All calculations were performed within the RMF approach and antiproton coupling constants were obtained by G-parity transformation. The possibility of annihilation of the antiproton in nuclear matter was not considered in this work.

Keywords: antiproton, RMF model, G-parity, atomic nucleus, nucelar density, single-particle energy

Názov práce: **Interakcia antiprotónov s jadrami**
Autor: Jaroslava Hrtánková

Katedra: Katedra Fyziky FJFI ČVUT v Prahe
Obor štúdia: Jadrové inžinierstvo
Druh práce: Bakalárska práca

Školiteľ: RNDr. Jiří Mareš, CSc.

Abstrakt: Cieľom tejto práce je skúmanie interakcie antiprotónu s jadrovou hmotou, najmä efekty silno interagujúceho antiprotónu na dynamiku nukleónov v jadrovej hmote. Táto práce najskôr zhŕňa základné poznatky o antičasticiach a vlastnostiach antiprotónu. Ďalej je stručne predstavená relativistická teória stredných polí (RMF) a je sformulovaný RMF model pre jadro s antiprotónom. Boli uskutočnené selfkonzistentné výpočty jednočasticových energií antiprotónu viazaného v ľahkom jadre kyslíku ^{16}O, ako aj výpočty energií a hustôt nukleónov. Dynamický prístup odhalil silné polarizačné efekty spôsobené prítomnosťou antiprotónu v jadre, t.j., veľké stlačenie jadrovej hmoty. Takisto sme zaznamenali obrovský nárast vo väzbovej energií systému $^{16}\mathrm{O} + \bar{p}$, okolo 1000 MeV. Všetky výpočty boli realizované v rámci RMF a väzbové konštanty pre antiprotón boli získané pomocou transformácie G-parity. V tejto práci ale nebola zahrnutá možnosť anihilácie antiprotónu v jadre.

Kľúčové slová: antiprotón, RMF model, G-parita, atómové jadro, jadrová hustota, jednočasticová energia

Prehlásenie

Prehlasujem, že som svoju bakalársku prácu vypracovala samostatne a použila som iba podklady (literatúru, projekty, SW atd.) uvedené v priloženom zozname.

Nemám závažný dôvod proti použitiu tohto školského diela v zmysle zákona §60 Zákona č.121/2000 Sb., o práve autorskom, o právach súvisiacich s právom autorským a o zmene niektorých zákonov (autorský zákon).

Declaration

I declare that I wrote my bachelor thesis independently and exclusively within the use of cited bibliography.

I agree with the usage of this thesis in the purport of the Act 121/2000 (Copyright Act).

V Prahe dňa ....

Jaroslava Hrtánková

Acknowledgement

I would like to thank my supervisor RNDr. Jiří Mareš, CSc. for his patience, willingness, and professional assistance during writing of this thesis. My great thanks belong to Ing. Daniel Gazda for his help with programming and for being ready to help when I needed it.

Contents

Chapter 1

Preface

This bachelor thesis deals with the study of the interaction of the antiproton with nuclei. The aim of this work is to explore the influence of the antiproton on surrounding nucleons. The study of the antiproton–nucleon and antiproton-nucleus interaction could test models of baryon–baryon interactions as well as nuclear models. The responses of a nucleus to the embedded antiproton can provide interesting information about nuclear dynamics, e.g., the information about the changes of the depth of a potential acting on nucleons in the presence of the antiproton. The issue of antiproton-nucleon annihilation is of interest as well. The interaction of the antiproton with nuclei is studied within a complex optical potential. Its imaginary part accounts for the absorption of the antiproton. The question is whether the antiproton can be attached at the periphery of a nucleus by a real attractive potential without being immediately absorbed. It has been shown that the deeply bound antiproton can theoretically exist in dense nuclear matter for relatively long time [1]. The annihilation can be realized by many channels producing mesons, even multinucleon annihilation is possible. The annihilation rates into different channels are proportional to the average available energy in phase space [2].

An important source of information about the antiproton–nucleus interaction is the experimental study of antiprotonic atoms. The antiprotonic atom is a sort of exotic hadronic atom that is created when a strongly interacting particle is captured by a target atom into an atomic orbit. The antiproton is much heavier than the electron and, therefore, gets much closer to the nucleus than the electron. Consequently, the antiproton feels not only the electromagnetic but also strong interaction. Due to this interaction the antiproton can be absorbed by the nucleus. This process is accompanied by the X-ray emission which provides valuable information about the energy shifts and widths of atomic levels [3].

The study of the interaction of the antiproton with a nucleus is performed in the framework of the relativistic mean-field (RMF) approach. This model was proposed

by Walecka in 1974 [4]. The RMF model describes nucleus as a system of Dirac nucleons interacting via boson fields. Many aspects of the nuclear structure and dynamics were successfully described within this approach (for references see e.g. [5]).

The Bachelor thesis is organized as follows: In the next chapter, the antiproton basic properties are introduced. The third chapter deals with the RMF model and equations of motion for nucleons and meson fields. The model for the description of a nuclear system with the antiproton is introduced in chapter 4. The results of our selfconsistent calculations of the ^{16}O nucleus with the antiproton are presented and discussed in chapter 5. Finally, conclusions are drawn in chapter 6.

Chapter 2

Antiproton and its properties

2.1 Antiparticles

In 1927, Paul Dirac derived an equation that described the motion of a free relativistic particle with half-integer spin. This equation had a rather strange implication. For every positive-energy solution there was a solution with negative energy. This would have meant, according to the tendency of every system to evolve in the direction of lower energy, that the particle should cascade into a negative state while radiating an infinite amount of energy (because there were infinitely many negative energy states available). To solve this problem Dirac postulated that the negative energy states are all filled by an infinite "sea" of fermions. The decay of particles from positive-energy states to negative energy states is then prohibited by the Pauli exclusion principle (which says that no two identical fermions may occupy the same quantum state simultaneously).

This new interpretation had an important consequence. If a photon with sufficient energy is absorbed by a negative energy particle, it results in the creation of a positive energy particle and a hole in the negative-energy "sea". This hole was interpreted as an antiparticle. Since the Dirac equation describes the motion of a fermion with spin 1/2, we would expect that for every known charged fermion there must exist its antifermion with the same mass and spin but opposite charge. Dirac's theory was confirmed by Anderson's discovery of the positron, a positively charged twin of an electron, in 1931. The development of quantum field theory, however, brought new insight into the hole theory. It has made the interpretation of antiparticles as holes in the vacuum unnecessary and the Dirac's theory has became a historical matter [6].

The antiparticles are standardly denoted by an overbar, for example, n is the neutron and $\bar{n}$ is the antineutron. It turns out that particles and their antiparticles

can generally differ not only in charge, but also in another quantum numbers like baryon and lepton number, strangeness, charm. This holds for fermions and so for bosons. In the case of neutral bosons with $B{=}L{=}S{=}C{=}0$, the antiparticle is identical with the particle, for instance, the photon $\gamma \equiv \bar{\gamma}$. The particle and its antiparticle have one specific feature. Since antiparticles have opposite additive quantum numbers from their particles, the quantum numbers of an annihilating pair are zero. Consequently, any set of particles whose total quantum numbers are zero could be produced, provided conservation of energy and momentum is obeyed (e.g. the annihilation could lead to photons or mesons). The laws of conservation guarantee that fermions are produced in pairs — particle and antiparticle.

In particle physics, there is a general principle called *crossing symmetry* [7]. Consider a reaction

$$A + B \to C + D. \tag{2.1}$$

We can "cross" over any particle to the other side of the equation and simultaneously replace the crossed particle with its antiparticle and vice versa. The new reaction will be also allowed. It can be, for example

$$A + \bar{C} \to \bar{B} + D. \tag{2.2}$$

This new reaction could be regarded as a different manifestation of the same fundamental process. However, there is one important restriction. If energy is not conserved, the process, otherwise permissible, will not occur.

2.2 Antiproton

The antiparticle of the proton is the antiproton, denoted by $\bar{p}$. The antiproton was first observed experimentally by Emilio Segré and Owen Chamberlain at Bevatron at University of California, Berkeley, in 1955 [8]. The laws of conservation allow the production of antinucleons only in pairs nucleon–antinucleon. The production of the antiproton is therefore allowed in reaction

$$p + p \to p + p + p + \bar{p}. \tag{2.3}$$

The threshold energy for production of antiprotons is about 6 GeV.

Antiprotons occur also in nature–they have been detected in cosmic rays. These cosmic antiprotons are produced in collisions of high energy protons with atomic nuclei in the interstellar medium.

The proton is a baryon and hence the antiproton is an antibaryon. Baryons

and antibaryons are strongly interacting particles–hadrons. In fact, baryons are not elementary particles. They have internal structure composed of quarks and gluons and interact strongly, electromagnetically and weakly. According to the quark model, the antiproton is composed of two up antiquarks and one down antiquark. The antiproton has the same mass and spin as the proton and all additive quantum numbers (such as charge, baryon number) have the same value with opposite sign. Selected properties of the antiproton and proton are compared in Table 2.1. The values are taken from ref. [9].

Table 2.1: Properties of antiproton and proton

	Antiproton	Proton
Mass (MeV)	938.272526(24)	938.272013(23)
Spin	1/2	1/2
Parity (-)	-1	+1
Mean life (years)	$>7 \times 10^5$	$>2.1 \times 10^{29}$
Electric charge (e)	-1	+1
Magnetic moment (μ_N)	-2.793(6)	2.792847356(23)
Baryon number (-)	-1	+1

The properties of the antiproton has been explored in many experiments. In 1986, antiprotons were first captured and stored in the Penning trap. These antiprotons were produced at LEAR (Low Energy Antiproton Ring) facility at CERN. Initial 21.3 MeV antiprotons were slowed down in kinetic energy by 4 orders of magnitude and then captured in a trap [10].

The antihydrogen atom $\bar{H}^0$, a bound state of the antiproton and positron, was first observed at LEAR in 1995 [11].

The OBELIX experiment in 1996 measured the cross section of proton–antiproton annihilation. The measurement was realized with low-momentum antiprotons (about 40 MeV). The data from this experiment confirmed the assumption that because of Coulomb attraction the cross-section behaves like $1/v^2$, where v is the velocity of the incident antiproton [12].

The experiment ASACUSA aims to study bound or continuum states of antiprotons in simple atoms [13]. In 2006 the ASACUSA experiment successfully determined the mass of the antiproton. The mass of the antiproton is 1836.153674 times the mass of the electron with an error of 5 in the last decimal place [14]. The corresponding mass of the proton is 1836.15367261 times the mass of the electron. These results confirm perfect agreement between the proton and antiproton masses.

2.2.1 Exotic atoms

An exotic atom is an atom in which an electron is replaced by another charged particle. It is formed whenever a charged particle from a beam enters an atomic target and is stopped in an atomic orbit replacing the electron. The exotic atom is usually formed in an excited state. The charged particle then cascades down through the atomic levels until it stops at some state with low principal quantum number n and then is absorbed by the nucleus. This process is accompanied by X-ray emission. Atoms with π^-, K^-, Σ^- or $\bar{p}$ are called hadronic atoms. The hadrons involved have long enough mean live times to study the strong interaction effects. Hadrons are much heavier then the electron, so they can get much closer to the atomic nucleus. As a consequence, their atomic orbital overlaps with the nucleus and they can interact strongly with the nucleons of the nucleus. The strong interaction of the hadron–nucleus system causes shifts (ε) and widths (Γ) of atomic levels and these are the subject of interest. The overlap of the hadron wave function with the nucleus covers a wide range of nuclear densities and can thus bring important information about the density dependence of the hadron–nucleus interaction. Moreover, hadronic atoms are an important source of information about the neutron density distribution in a nucleus [15].

The shifts and widths of energy levels in hadronic atoms have been measured already for several decades. Experiments with antiprotons were carried out at LEAR facility at CERN [16], kaonic atoms were studied at KEK [17] and DAΦNE (Frascati) [18].

The calculations of strong interaction effects are performed using an optical potential which is added to the Coulomb interaction. The simplest form of the optical potential is given by

$$V_{opt} = t\rho, \tag{2.4}$$

where t is the two-body hadron-nucleon scattering amplitude and ρ is the nuclear density distribution. As can be seen, the optical potential is density dependent. The density distribution of protons is considered to be known. It is obtained from the finite nuclear charge distribution [19]. However, there is no sufficient information about the neutron density distribution with required accuracy. Experiments with pionic atoms revealed [20] that the main feature of the neutron density which influences strong interaction effects is its radial extent. The shape of the neutron density distribution and other features are less important. Therefore, the dependence of the difference of rms radii $r_n - r_p$ on $(N - Z)/A$ has been studied in hadronic atoms [15].

The experimental information about the strong interaction effects in antiprotonic

atoms consists of 90 points of X-ray data and 17 points of radiochemical data [15]. The radiochemical method is based on measuring activities of residual nuclei which are produced by annihilation of $\bar{p}$ on a single peripheral nucleon. This measurement can provide the ratio between the probability of annihilation of $\bar{p}$ on a neutron to that on a proton. Considering the fact that the annihilation takes place in the surface region of nuclei, it gives information on the ratios between the neutron and proton densities in this region. The combination of these two types of data leads to consistent results as shown in ref. [21].

The study of antiprotonic atoms revealed a large cross-section for annihilation of antiprotons on nucleons. This implies a large value of the imaginary part of the optical potential of the order of 100 MeV. The absorption takes place mainly at the surface of the nucleus and, therefore, $\bar{p}$ hardly penetrates deep into the nuclear interior. This fact considerably complicates the connection between the free $\bar{p}$N interaction and the interaction inside nuclear matter. For more details see [3, 21, 15].

Chapter 3

Relativistic mean-field approach

In the framework of the relativistic mean-field theory, nucleons are described as Dirac fields ψ which interact by the strong interaction mediated by meson exchange. The mesons are also treated as fields. These are sorted by their internal angular momentum J, parity Π and isospin I. Only the fields with good parity are considered because we are working with nuclear states with natural parity. The formalism includes the following fields: isoscalar-scalar field $\sigma(x^\mu)$ (σ), isoscalar-vector field $\omega_\mu(x^\mu)$ (ω), isovector-vector field $\vec{\rho}_\mu(x^\mu)$ (ρ) and massless vector field $A_\mu(x^\mu)$ (γ). The σ-field is responsible for the medium range attraction between nucleons, the ω-field mediates the short range repulsion, the ρ-field allows to adjust isovector properties of the studied nuclear systems and the photon mediates the electromagnetic interaction. The mean-field theory is based on two approximations which allow us to solve the equations of motion for the above mentioned fields. These are the *mean-field* approximation and the *no-sea* approximation [22].

3.1 Mean-field approximation

The mean-field approximation is based on substituting the quantum fields by their expectation values. This means that all quantum fluctuations are dismissed and quantum fields are treated as c-number fields. This approximation simplifies handling with nucleons which are then moving as independent particles in the meson mean fields. For example, consider a system consisting of nucleons ψ which interact only by the scalar field σ. The Lagrangian density for this system is

$$\mathscr{L} = \bar{\psi}(i\gamma^\mu\partial_\mu - m_N)\psi + \frac{1}{2}(\partial^\mu\sigma\partial_\mu\sigma - m_\sigma^2\sigma^2) - g_\sigma\bar{\psi}\psi\sigma. \tag{3.1}$$

Here, the meson field operator is replaced by its expectation value

$$\hat{\sigma} \rightarrow \sigma = \langle \sigma \rangle, \tag{3.2}$$

therefore all nucleons interact only via the σ meson mean field.

3.2 No-sea approximation

Since the nucleons move as independent particles in this model, the nucleon field operator can be expanded at all times in terms of single particle states α as

$$\hat{\psi} = \sum_{\alpha} \psi_{\alpha}(x^{\mu}) \hat{a}_{\alpha}, \tag{3.3}$$

where $\hat{a}_{\alpha}$ is the annihilation operator for a nucleon in the state α and $\psi_{\alpha}(x^{\mu})$ is the single particle wave function. For example, the scalar density can be written in the form

$$\langle : \bar{\psi}\psi : \rangle = \rho_{vacuum} + \sum_{\alpha=1}^{A} \bar{\psi}_{\alpha}\psi_{\alpha}, \tag{3.4}$$

where $: \cdots :$ symbolizes the normal ordered product, i.e., all creation operators are moved to the left of annihilation operators, ρ_{vacuum} denotes the contribution from vacuum polarization and second term denotes the contribution of A nucleons bound in a nucleus. The no-sea approximation consists in neglecting the contribution from the vacuum. More detailed explanation is given in ref. [22].

3.3 RMF model

We will consider all aforementioned nucleon and meson fields. The Lagrangian density of the RMF model for nucleons and mesons has the form

$$\begin{aligned}
\mathscr{L} =& \bar{\psi}(i\gamma^{\mu}\partial_{\mu} - m_N)\psi \\
&+ \frac{1}{2}\partial_{\mu}\sigma\partial^{\mu}\sigma - \frac{1}{2}m_{\sigma}^2\sigma^2 - g_{\sigma N}\bar{\psi}\psi\sigma - \frac{1}{3}g_2\sigma^3 - \frac{1}{4}g_3\sigma^4 \\
&- \frac{1}{4}\Omega_{\mu\nu}\Omega^{\mu\nu} + \frac{1}{2}m_{\omega}^2\omega^{\mu}\omega_{\mu} - g_{\omega N}\psi\gamma_{\mu}\psi\omega^{\mu} + \frac{1}{4}d(\omega^{\mu}\omega_{\mu})^2 \\
&- \frac{1}{4}\vec{R}_{\mu\nu} \cdot \vec{R}^{\mu\nu} + \frac{1}{2}m_{\rho}^2\vec{\rho}_{\mu} \cdot \vec{\rho}^{\mu} - g_{\rho N}\bar{\psi}\gamma_{\mu}\vec{\tau}\psi \cdot \vec{\rho}^{\mu} \\
&- \frac{1}{4}F_{\mu\nu}F^{\mu\nu} - e\bar{\psi}\gamma_{\mu}\frac{1}{2}(1+\tau_3)\psi A^{\mu},
\end{aligned} \tag{3.5}$$

where the arrow denotes isovector quantity and $\vec{\tau}$ is the triplet of Pauli matrices; m_N, m_σ, m_ω, m_ρ are the masses of nucleon, σ-, ω- and ρ-meson; $g_{\sigma N}$, $g_{\omega N}$, $g_{\rho N}$ and e are the coupling constants of the corresponding fields to the nucleon. The field tensors are defined as

$$\begin{aligned}
\Omega_{\mu\nu} &= \partial_\mu \omega_\nu - \partial_\nu \omega_\mu \\
\vec{R}_{\mu\nu} &= \partial_\mu \vec{\rho}_\nu - \partial_\nu \vec{\rho}_\mu - g_{\rho N}(\vec{\rho}_\mu \times \vec{\rho}_\nu) \\
F_{\mu\nu} &= \partial_\mu A_\nu - \partial_\nu A_\mu.
\end{aligned} \tag{3.6}$$

We consider stationary states of spherical symmetric nuclei. We will look for the solution of the Dirac equation in the form

$$\psi_i(x) = e^{-i\epsilon_i t}\psi_i(\vec{x}). \tag{3.7}$$

It implies that all time derivatives of the fields vanish and all spatial components of the fields will be zero as well

$$\dot{\sigma} = 0, \quad \dot{\omega}_\mu = 0, \quad \dot{\vec{\rho}}_\mu = 0, \quad \dot{A}_\mu = 0 \tag{3.8}$$

$$\langle \omega_i \rangle = 0, \quad \langle \vec{\rho}_i \rangle = 0, \quad \langle A_i \rangle = 0 \quad \text{for } i\text{=1,2,3.} \tag{3.9}$$

Rotational invariance causes that all the fields will depend only on the radial coordinate r. We further assume that the nucleon single particle states do not mix isospin, so only the third neutral component of the isovector meson ρ is considered. Only the fields σ, ω_0, ρ_0 and A_0 remain after the above simplifications. As a result, the Lagrangian density (3.5) will acquire the form

$$\begin{aligned}
\mathscr{L}_{RMF} =& \bar{\psi}_i(i\gamma_\mu\partial^\mu - m_N - g_{\sigma N}\sigma_0 - g_{\omega N}\gamma_0\omega_0 - g_{\rho N}\gamma_0\tau_3\rho_0 - e\gamma_0\frac{1+\tau_3}{2}A_0)\psi_i \\
&- \frac{1}{3}g_2\sigma_0^3 - \frac{1}{4}g_3\sigma_0^4 + \frac{1}{4}d\omega_0^4 - \frac{1}{2}[(\nabla_i\sigma_0)^2 + m_\sigma^2\sigma_0^2] \\
&+ \frac{1}{2}[(\nabla_i\omega_0)^2 + m_\omega^2\omega_0^2] + \frac{1}{2}[(\nabla_i\rho_0)^2 + m_\rho^2\rho_0^2] + \frac{1}{2}(\nabla_i A_0)^2.
\end{aligned} \tag{3.10}$$

Using the Hamilton's variational principle we find Euler-Lagrange equations for the motion of a given field $\phi(\vec{x},t) = \psi_i, \sigma, \omega, \rho, A$

$$\frac{\partial\mathscr{L}}{\partial\phi(x)} - \frac{\partial}{\partial x^\mu}\frac{\partial\mathscr{L}}{\partial(\partial_\mu\phi)} = 0. \tag{3.11}$$

Applying the Euler-Lagrange equations (3.11) to the RMF Lagrangian (3.10) we obtain Dirac equations of motion for nucleons

$$[-i\alpha_j\nabla_j + \beta(m + g_{\sigma N}\sigma) + g_{\omega N}\omega_0 + g_{\rho N}\rho_0\tau_3 + e\frac{1+\tau_3}{2}A_0]\psi_i = \epsilon_i\psi_i. \tag{3.12}$$

The meson field equations of motion in the mean-field approximation are

$$(-\triangle + m_\sigma^2 + g_2\sigma + g_3\sigma^2)\sigma = -g_{\sigma N}\rho_S \tag{3.13}$$

$$(-\triangle + m_\omega^2 + d\omega_0^2)\omega_0 = g_{\omega N}\rho_V \tag{3.14}$$

$$(-\triangle + m_\rho^2)\rho_0 = g_{\rho N}\rho_I \tag{3.15}$$

$$-\triangle A_0 = e\rho_p. \tag{3.16}$$

The corresponding densities are defined as

$$\rho_S = \sum_{i=1}^{A}\bar{\psi}_i\psi_i \tag{3.17}$$

$$\rho_V = \sum_{i=1}^{A}\bar{\psi}_i\beta\psi_i \tag{3.18}$$

$$\rho_I = \sum_{i=1}^{A}\bar{\psi}_i\beta\tau_3\psi_i \tag{3.19}$$

$$\rho_p = \sum_{i=1}^{A}\bar{\psi}_i\beta\frac{1+\tau_3}{2}\psi_i, \tag{3.20}$$

where the sums run over all occupied single-particle states.

Chapter 4

$\bar{\text{p}}$-nucleus interaction

4.1 Antibaryon–nucleus interaction

The interaction of antibaryons with nuclei is an interesting topic. Unfortunately, only a little is known about it. The main source of information is the study of antiproton atoms and $\bar{p}$-scattering experiments. The possibility of forming a bound state of the antinucleon in a nucleus was first studied in the 80s [23, 24].

The charge independence of the strong interaction led to the introduction of isospin. Projections of I correspond to different particle charge states. The combination of charge conjugation (see below) and rotation in isospin space gives the transformation

$$\hat{G} = \hat{C}e^{i\pi I_1} \tag{4.1}$$

called G-parity. The symbol I_1 is the generator of rotation around 1-axis and $\hat{C}$ is the charge conjugation operator. The eigenstates of $\hat{G}$-parity operator are, for example, charged mesons (even though they are not eigenstates of $\hat{C}$ alone). Multiplet with the isospin I has the eigenvalue

$$\hat{G}|I\rangle = (-1)^I C|I\rangle, \tag{4.2}$$

where C is the charge conjugation number of the neutral member (e.g. π^0). G-parity is a multiplicative quantum number; for a system of n pions the eigenvalue is $(-1)^n$. If the Hamiltonian of a system is invariant under charge conjugation and rotation in isospin space, the G-parity is conserved.

Charge conjugation, $\hat{C}$, is a transformation, which converts a particle into its antiparticle. It means that it reverses sign of the charge, baryon number, lepton number, strangeness, charm, beauty, truth ... On the other hand, it does not change

mass, momentum, energy, and spin. Therefore it holds

$$\hat{C}|p\rangle = |\bar{p}\rangle, \tag{4.3}$$

where $|p\rangle$ ($|\bar{p}\rangle$) denotes some state of a particle (antiparticle). Double application of $\hat{C}$ turns the system back to the initial state. As a consequence, the eigenvalues of $\hat{C}$ are ± 1. However, not every particle is the eigenstate of the operator $\hat{C}$. In fact, only particles identical with their antiparticles can be eigenstates of the charge conjugation operator. Such particles are, for example, photon or π^0 meson. A system of particles, like a bound state of fermions and antifermions, with total angular momentum l and spin s, constitutes the eigenstate of $\hat{C}$ with the eigenvalue $(-1)^{l+s}$. Using this prescription, the charge conjugation number C of mesons can be determined from the quark model.

The G-parity transformation thus inverts the nucleon into the antinucleon. Therefore, the potential for the antiproton can be obtained by the transformation of the proton potential

$$V_{\bar{p}} = \hat{G}V_p\hat{G} = G_\sigma V_\sigma + G_\omega V_\omega + G_\rho V_\rho + G_\gamma V_\gamma, \tag{4.4}$$

where the symbols G_σ, G_ω, G_ρ and G_γ denote the value of G-parity for the meson and photon fields. The fields σ, ρ and Coulomb field have positive G-parity. In contrast, the ω meson has negative G-parity. Expressing this by coupling constants gives

$$g_{\sigma\overline{N}} = g_{\sigma N}, \quad g_{\omega\overline{N}} = -g_{\omega N}, \quad g_{\rho\overline{N}} = g_{\rho N}\ . \tag{4.5}$$

The nuclear ground state is well described by an attractive scalar potential of magnitude $|S| \simeq 350$ MeV and a repulsive vector potential $|V| \simeq 300$ MeV. The central potential for slow nucleons is then $S + V \simeq -50$ MeV. For antinucleons the vector potential changes sign and consequently the central potential becomes very deep, $S - V \simeq -650$ MeV. The presence of antiproton in a nucleus causes significant changes in its structure. Because of the very deep $\bar{p}$ potential the binding energy of the nucleus with antiproton considerably increases and so does the central density of the system.

Of course, the relations for the coupling constants (4.5) is an idealization. There are several factors which can modify the meson fields like many-body effects and $\bar{p}$-annihilation. The G-parity may be violated in dense baryon-rich matter when the quark-antiquark degrees of freedom start to play a role. The maximal binding energy per quark-antiquark pair in baryon-symmetric matter predicted by Nambu-Jona-Lasinio (NJL) model [25] is about five times lower than within the RMF model

(for more details see ref. [2]). This violation may cause that the value of coupling constants for the antiproton (4.5) are overestimated. Therefore, we considered also the reduced antiproton coupling constants

$$g_{\sigma\bar{p}} = \xi\, g_{\sigma N}, \quad g_{\omega\bar{p}} = -\xi\, g_{\omega N}, \quad g_{\rho\bar{p}} = \xi\, g_{\rho N}\ , \tag{4.6}$$

where the scaling parameter ξ is from interval $\langle 0, 1\rangle$ and is considered to have the same value for all fields.

The value of the parameter ξ could be determined from fits to atomic data. Such fits to a large database were performed by Friedman et al. in 2005 [15]. It was found that the value of the parameter ξ varies between 0.15 (^{40}Ca) and 0.35 (^{208}Pb). So there is a substantial deviation from the G-parity transformed $\bar{p}$-coupling constants.

4.2 RMF model for nucleus with antiproton

In the framework of the RMF model, the antiproton interacts with nucleons through the exchange of the scalar (σ) and vector (ω, ρ) mesons and photon field (γ). The Dirac equations for the antiproton and nucleons ($i = N, \bar{p}$) will have the form

$$[-i\alpha_j \nabla_j + \beta(m_i + S_i) + V_i]\psi_i = \epsilon_i \psi_i, \tag{4.7}$$

where

$$S_i = g_{\sigma i}\sigma, \quad V_i = g_{\omega i}\omega_0 + g_{\rho i}\rho_0\tau_3 + e_i\frac{1+\tau_3}{2}A_0. \tag{4.8}$$

The Klein-Gordon equations for the meson fields will be modified due to the presence of the antiproton as follows:

$$(-\triangle + m_\sigma^2 + g_2\sigma + g_3\sigma^2)\sigma = -g_{\sigma N}\rho_S - \xi\, g_{\sigma N}\rho_{S\bar{p}} \tag{4.9}$$

$$(-\triangle + m_\omega^2 + d\omega_0^2)\omega_0 = g_{\omega N}\rho_V - \xi\, g_{\omega N}\rho_{V\bar{p}} \tag{4.10}$$

$$(-\triangle + m_\rho^2)\rho_0 = g_{\rho N}\rho_I + \xi\, g_{\rho N}\rho_{I\bar{p}} \tag{4.11}$$

$$-\triangle A_0 = e\rho_p - e\rho_{\bar{p}}. \tag{4.12}$$

The equations of motion are solved numerically by an iteration procedure. The solution is described in detail in ref. [26]. The binding energy of the system is

determined by

$$
\begin{aligned}
B(A,Z,\bar{p}) = & \textstyle\sum_{i=1}^{A}(m_N-\epsilon_i)+(m_{\bar{p}}-\epsilon_{\bar{p}}) \\
& -\frac{1}{2}\int \mathrm{d}^3x\,(-g_{\sigma N}\,\sigma\rho_S+g_{\omega N}\,\omega_0\rho_V+g_{\rho N}\,\rho_0\rho_I+e\,A_0\rho_p) \\
& -\frac{1}{2}\int \mathrm{d}^3x\,(-\tfrac{1}{3}g_2\,\sigma^3-\tfrac{1}{2}g_3\,\sigma^4+\tfrac{1}{2}d\,\omega^4) \\
& -\frac{1}{2}\int \mathrm{d}^3x\,(-g_{\sigma\bar{p}}\,\sigma\rho_{S\bar{p}}+g_{\omega\bar{p}}\,\omega_0\rho_{V\bar{p}}+g_{\rho\bar{p}}\,\rho_0\rho_{I\bar{p}}-e\,A_0\rho_{\bar{p}})\,.
\end{aligned}
\tag{4.13}
$$

4.3 RMF Parametrization

There exist several parameter sets for the RMF model, which define the masses of meson fields and the values of their coupling constants. These parametrizations are divided into so called linear and nonlinear models. The linear models have advantage in their simplicity and numerical stability. They describe rms radii, nuclear densities and single particle energies quite well. But the linear parametrizations give nuclear compressibility K too large. The nonlinear models contain extra nonlinear terms for the scalar field σ and the vector field ω. These models give much better binding energies of nuclei and also fit better other experimental data. The detailed description is given in ref. [22].

Table 4.1: The parameters of TM2 and HS model

	TM2	HS
m_N[MeV]	938	939
m_σ [MeV]	526.443	520
m_ω [MeV]	783	783
m_ρ [MeV]	770	770
$g_{\sigma N}$	11.4694	10.47
$g_{\omega N}$	14.6377	13.8
$g_{\rho N}$	9.3566	8.07
g_2 [fm^{-1}]	-4.444	0
g_3	4.6076	0
d	84.5318	0

In this work, two models, namely TM2 and HS, were adopted. The TM2 parametrization was introduced by Sugahara and Toki [27]. The TM2 parametrization is nonlinear and contains an extra nonlinear term ω^4. The corresponding coupling constant is denoted by d. The TM2 model was inspired by the relativistic Brueckner-Hartree-Fock (RBHF) theory of nuclear matter. The reason for introducing the nonlinear term ω^4 lies in the weakening of the vector potential from

linear behavior at high densities in order to get closer to the results of the RBHF theory. This model gives the value of the compressibility $K = 344$ MeV.

The HS parametrization is a linear parametrization introduced by Horowitz and Serot [28]. This model gives very large value of nuclear compressibility, $K = 544.4$ MeV. Parameters of the TM2 and HS RMF models are listed in Table 4.1.

Chapter 5

Results

In this work, the properties of the ^{16}O nucleus with one added antiproton were explored. The ^{16}O nucleus is a light magic nucleus, which is suitable for the RMF approach. Magic nuclei are characterized by the high binding energy per nucleon and high stability. Within the shell model magic nuclei have all their shells closed (filled) and they are spherical.

I performed calculations of the densities and energies in ^{16}O plus one proton in $1s_{1/2}$ state and for ^{16}O plus one antiproton in $1s_{1/2}$ state. I will use notation $^{16}O_p$ for ^{16}O plus one proton in $1s_{1/2}$ and $^{16}O_{\bar{p}}$ for ^{16}O plus one antiproton. Of course, the ^{16}O nucleus plus one proton in $1s_{1/2}$ state cannot exist in real world because of the Pauli exclusion principle. I used this fictitious system as a tool for testing the model and numerical code. The antiproton could be also added into the states characterized by higher quantum numbers. It would be interesting to explore such states as well but this was not in the center of my interest in this work.

I used the set of coupling constants (4.6) for the antiproton. To be more specific, I did calculations for the values of $\xi = 0.25, 0.5, 0.75$ and 1. The vast majority of the calculations were performed dynamically, i.e, the nucleus was allowed to change its rearrangement due to the presence of the antiproton. For comparison, I did also static calculations, i.e. the nuclear core was not allowed to response to the presence of the antiproton, for a comparison between the dynamical and static approach.

The presence of the antiproton in a nucleus causes considerable changes in the magnitudes of the scalar and vector potentials. In Figure 5.1, the scalar and vector potentials felt by the antiproton in the $^{16}O_{\bar{p}}$ system are shown as a function of r. The scalar and vector potentials in $^{16}O_p$ are shown for comparison. The extra proton in the $1s_{1/2}$ state causes small changes of the scalar and vector potentials. Moreover, these changes are approximately the same in the both cases. On the other hand, the addition of the antiproton results in a significant increase of the scalar (attractive)

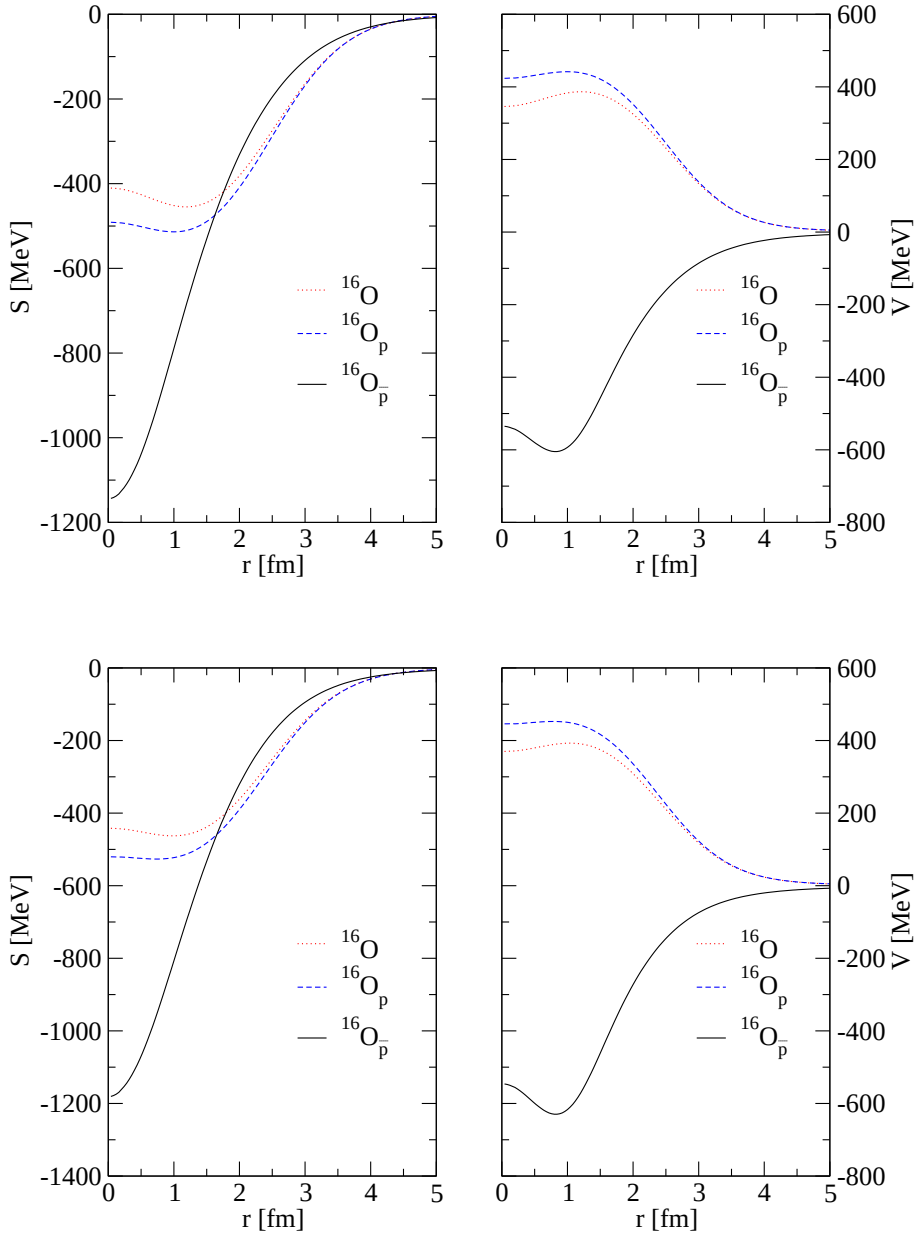

Figure 5.1: The scalar (left) and vector (right) potentials in the ^{16}O nucleus felt by protons in comparison with potentials in the nucleus $^{16}\mathrm{O}_p$ and the potentials in the $^{16}\mathrm{O}_{\bar{p}}$ nucleus for the antiproton. The results for the TM2 model (top) and the HS model (bottom) are presented for comparison.

potential. Due to the G-parity transformation, the vector potential reverses its sign and becomes attractive too. However, its depth is about half of the depth of the scalar potential. Protons and neutrons also feel much stronger attraction due to the presence of antiproton in the nucleus (of course, the vector potential is repulsive for nucleons).

The density distributions of the core nucleons in ^{16}O and $^{16}\mathrm{O}_{\bar{p}}$ are displayed in

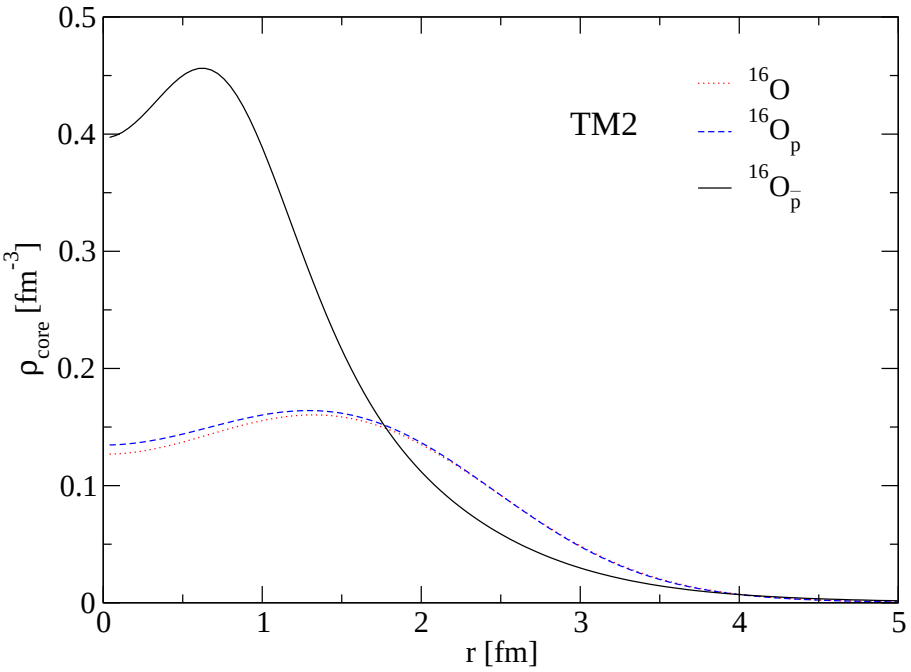

Figure 5.2: The density distribution of the nuclear core of $^{16}O_{\bar{p}}$ compared with the nuclear density in ^{16}O and the density distribution of the core in $^{16}O_p$, for the TM2 model.

Figure 5.2. We witness a huge increase of the core density in $^{16}O_{\bar{p}}$. The central density is about three times larger than the density in ^{16}O. The addition of the $1s_{1/2}$ proton into the ^{16}O nucleus causes only a minor increase of the density of the core.

In Figure 5.3, the density distribution of nucleons in $^{16}O_{\bar{p}}$ are displayed for different values of the scaling factor ξ. The central density of nucleons grows with increasing value of the parameter ξ. There is a considerable increase of the density in the center of the nucleus for $\xi = 0.25$. However, the density increases until the critical value $\xi = 0.75$, when it starts to decrease. We observed some sort of saturation of the nucleon density. This can be caused by the increase of the repulsive ω field between nucleons of the core and by shell effects.

The core nucleons are compressed due to the presence of the antiproton and their single particle energies increase as well. The extent of the rearrangement of the nuclear core is connected with the nuclear compressibility. Indeed, larger polarization effects are predicted by the TM2 model which gives lower value of the nuclear compressibility than the HS model.

The density distribution of the antiproton in the ^{16}O nucleus is presented in Figure 5.4. The density of the antiproton calculated statically within the TM2 model is about half of the density of the antiproton calculated dynamically. In the static approach nucleons are not compressed as the nuclear core is not allowed to

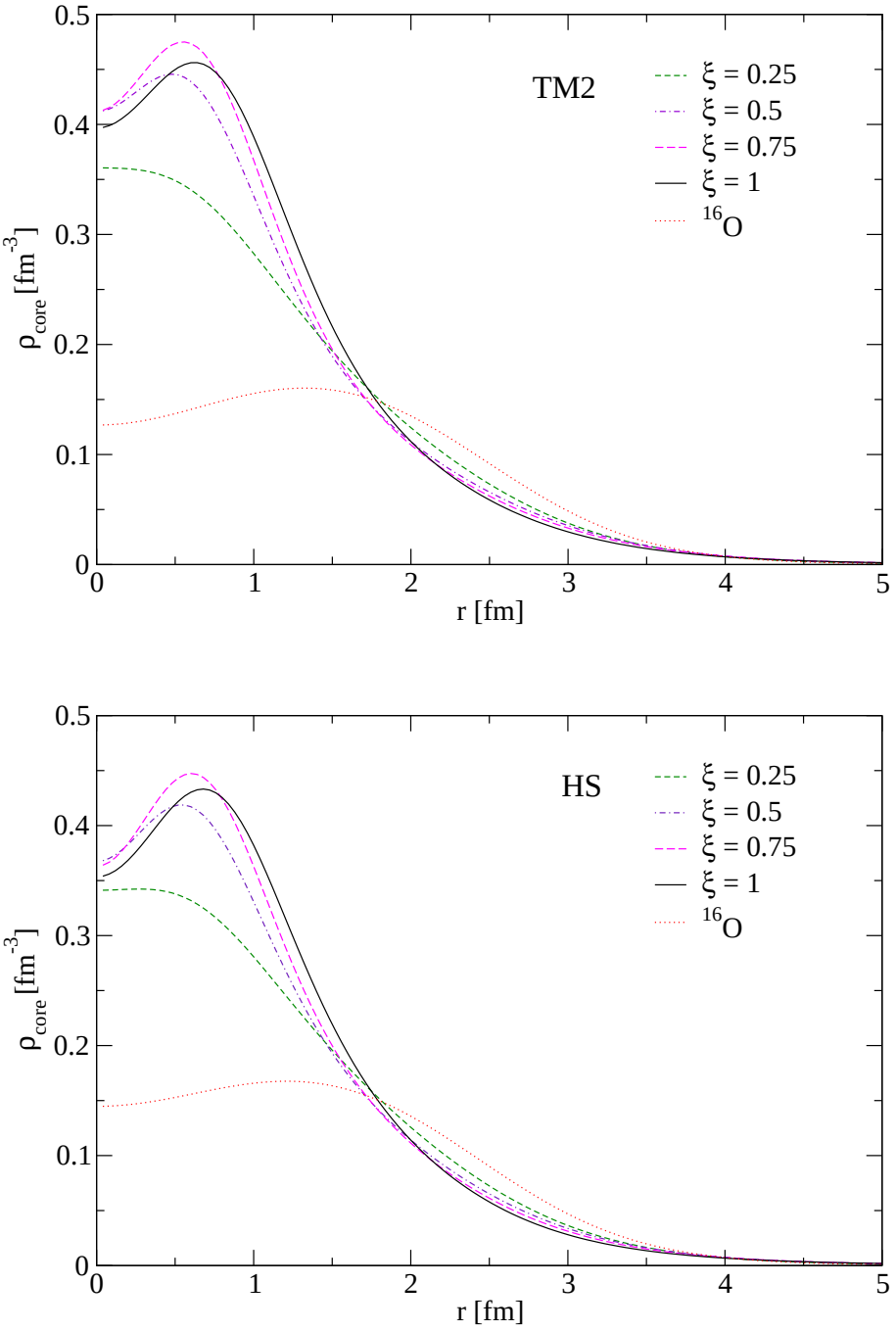

Figure 5.3: The density of nucleons in $^{16}O_{\bar{p}}$ for different values of the parameter ξ in comparison with the density of ^{16}O within the TM2 (top) and the HS (bottom) model.

be polarized by the extra antiproton. In the case of the antiproton density we can again see the effect of saturation. But now, it occurs for the value of $\xi = 0.5$. Then the antiproton density rapidly decreases, and for $\xi = 1$ it becomes more flat in the center. This is an indication that shell effects control the structure of the nuclear system with an antiproton and consequently the $\bar{p}$ density distribution. For the HS

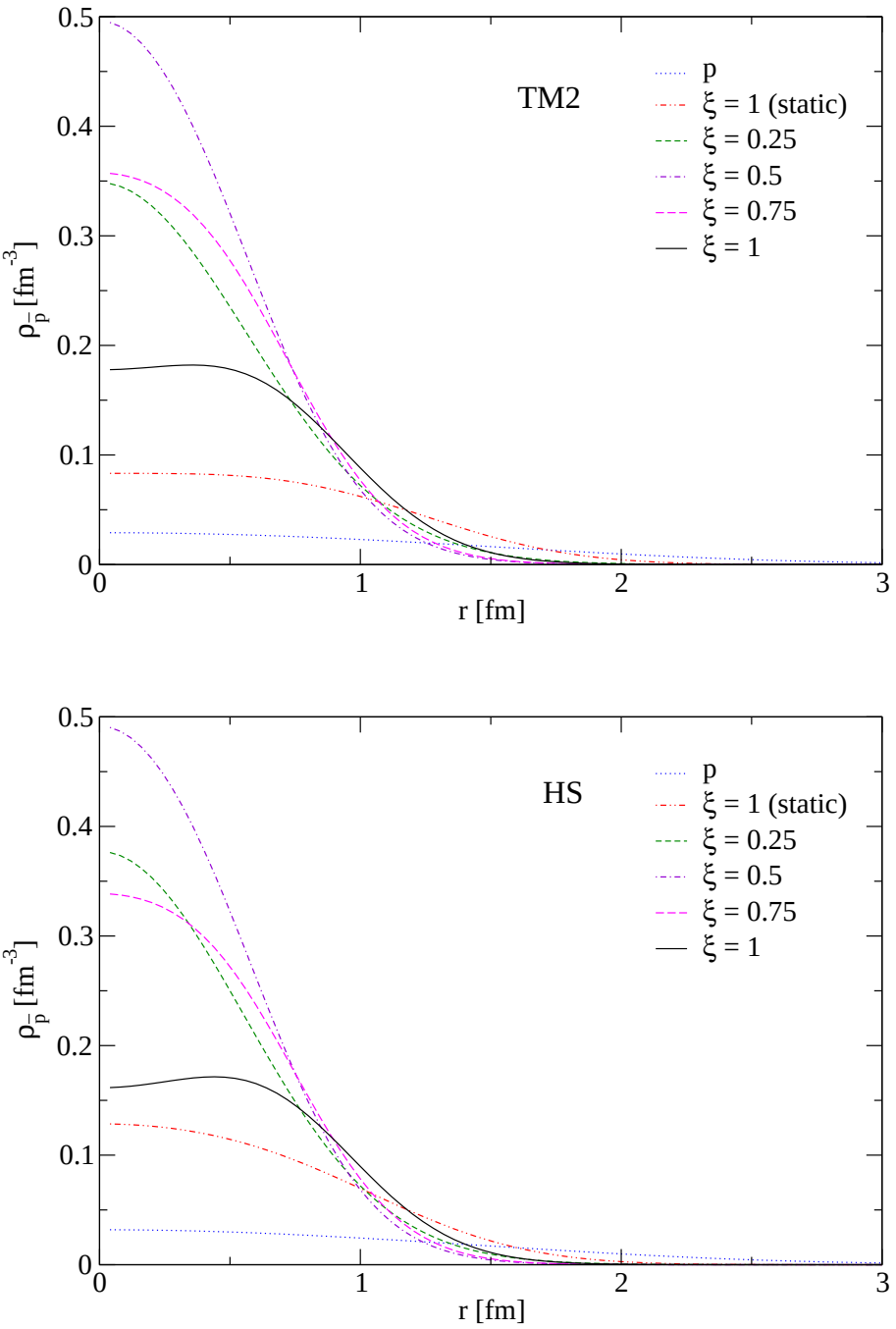

Figure 5.4: The density of antiproton in $^{16}O_{\bar{p}}$ for different values of the parameter ξ in comparison with the density of the $1s_{1/2}$ proton in $^{16}O_p$, for the TM2 (top) and the HS (bottom) model. The $\bar{p}$ density in $^{16}O_{\bar{p}}$ calculated statically for $\xi = 1$ is shown for illustration.

model, the difference between the dynamic and static approaches is not so large. There is a larger increase in the antiproton density for $\xi = 0.25$ then for the TM2 model. The saturation value is again at $\xi = 0.5$. The decrease of the antiproton density in the HS model is more pronounced than within the TM2 model.

In Figure 5.5, the densities of protons and neutrons in the $^{16}O_{\bar{p}}$ nucleus are displayed separately as a function of r. The saturation of the proton and neutron densities is again obvious . The density of protons is higher than the density of neutrons. This can be explained by the fact that protons feel in addition the Coulomb and isovector attraction from the antiproton. The densities are higher within the TM2 model because of lower compressibility of the nuclear matter than in the HS model.

The difference between proton and neutron densities is more obvious from Figure 5.6 where the difference $\triangle\rho = \rho_p - \rho_n$ is plotted as function of r. The largest difference is between the proton and neutron densities in the case of $\xi = 0.75$ for both parametrizations. The figure shows that protons are more concentrated in the center of $^{16}O_{\bar{p}}$ than neutrons. On the contrary, the difference between the proton and neutron densities in ^{16}O (dotted line) is negative because the central density of neutrons is higher than the central density of protons. This is another example of the sizeable rearrangement of the nuclear core of the $^{16}O_{\bar{p}}$.

The energies of the antiproton are displayed in Figure 5.7. The energy of the antiproton increases gradually as the potential increases with the parameter ξ. The antiproton is more bound within the HS model because this model gives stronger mean fields than TM2, and, consequently, a deeper potential for the antiproton. But the difference between both models is relatively small. For $\xi = 1$, the single particle energy of the antiproton reaches the value of 1212.38 MeV within the TM2 model and 1240.76 MeV within the HS model. The static approach gives for $\xi = 1$ the value of 755.85 MeV and 765.15 MeV in the TM2 and HS model, respectively. Figure 5.7 illustrates again the important role of the rearrangement of the nuclear core and the necessity of performing dynamical calculations.

The single-particle energies of nucleons in a nucleus with the antiproton increase as well. Figure 5.8 shows the energy levels for protons and neutrons in the $^{16}O_{\bar{p}}$ system, calculated for $\xi = 1$. Protons in the $1s_{1/2}$ state are bound most strongly since they feel in addition stronger attraction due to the Coulomb and isovector field. On the contrary, neutrons feel a repulsive isovector field due to the antiproton since they have the same isospin projection. As a result, they are less bound than protons in $^{16}O_{\bar{p}}$. Both models predict a considerable increase of the proton and neutron level spacing between the s and p levels. This huge s-p level spacing is a consequence of a much deeper and narrower potential well in $^{16}O_{\bar{p}}$ than in ordinary ^{16}O nucleus. The nucleon p states are affected by the presence of the antiproton in a nucleus much less than the s state. It is due to the smaller range of the nuclear potential and, in the case of $1p_{1/2}$, also due to the spin-orbit interaction. The spin-orbit splitting of the $1p_{3/2}$ and $1p_{1/2}$ states in $^{16}O_{\bar{p}}$ is much larger than in ^{16}O. The spin-orbit interaction

is proportional to the sum of the absolute values of the scalar and vector potentials. In the case of $^{16}O_{\bar{p}}$, this sum is much larger than in the ordinary ^{16}O nucleus. As a result, the $1p_{1/2}$ state in $^{16}O_{\bar{p}}$ lies even higher than in ^{16}O.

The total binding energy of $^{16}O_{\bar{p}}$ reaches the value of 1259.88 MeV within the TM2 model and the value of 1247.21 MeV within the HS model. For comparison, the binding energy of the ^{16}O nucleus is 128.6 MeV and 90.16 MeV within the TM2 and HS model, respectively. The increase of the binding energy is higher for the HS model because of the stronger mean fields involved. But the differences are not so large. We can conclude that the both models give similar results.

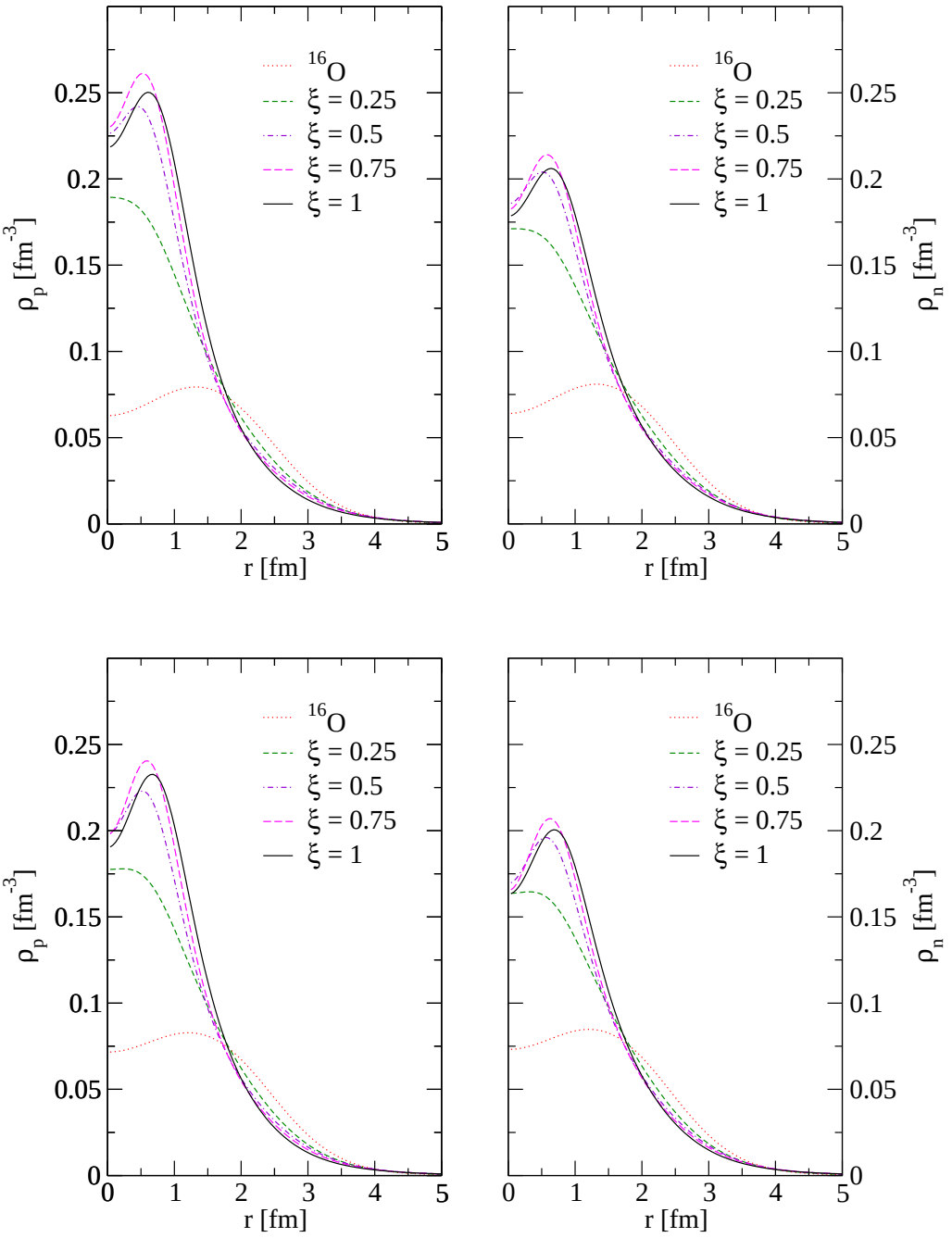

Figure 5.5: The density of protons (left) and neutrons (right) in $^{16}O_{\bar{p}}$ for different values of the parameter ξ in comparison with the density of protons and neutrons in ^{16}O within the TM2 (top) and the HS (bottom) model.

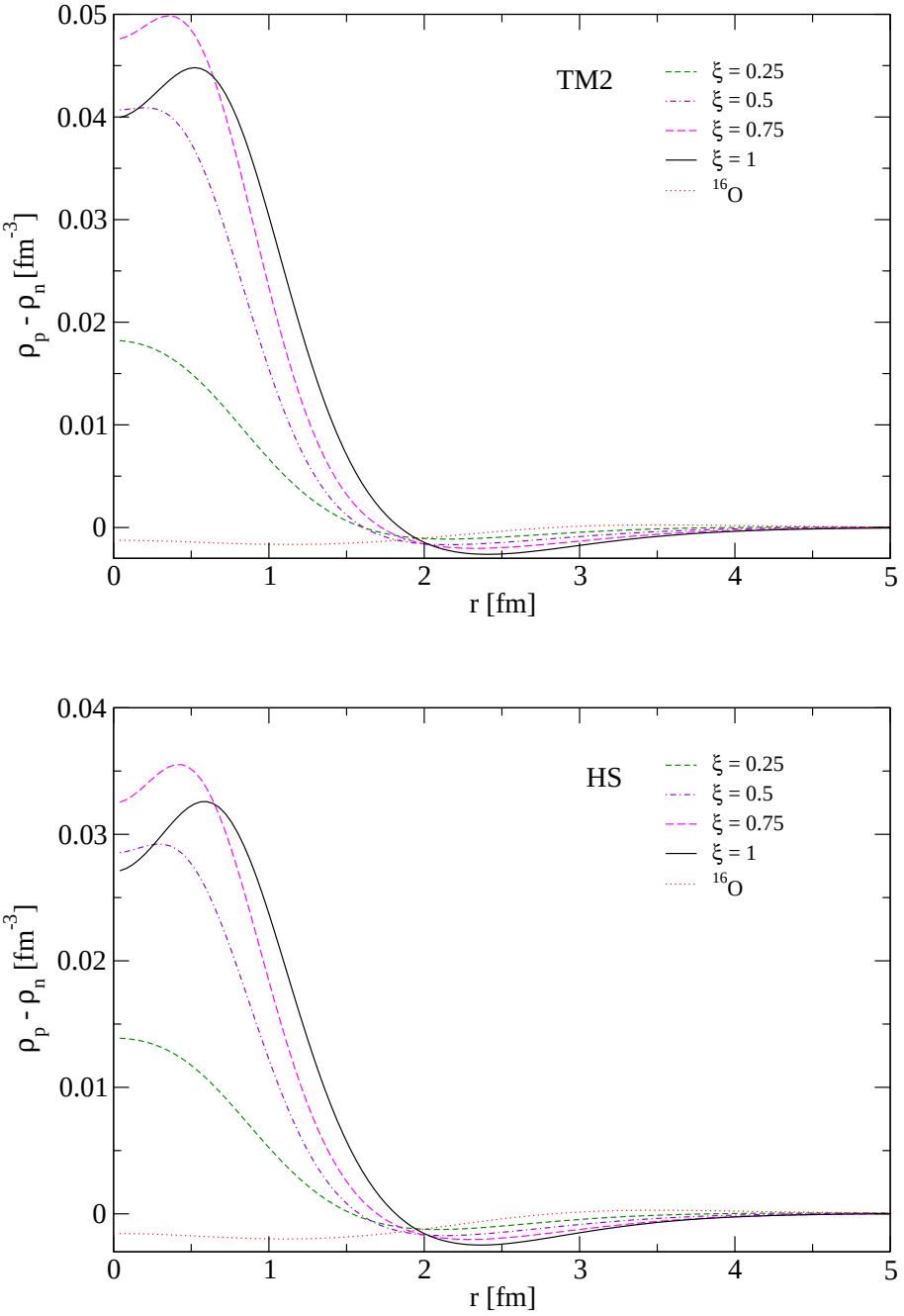

Figure 5.6: The difference between the proton and neutron density $\triangle\rho = \rho_p - \rho_n$ in $^{16}O_{\bar{p}}$ for given parameters ξ in the TM2 (top) and HS (bottom) model.

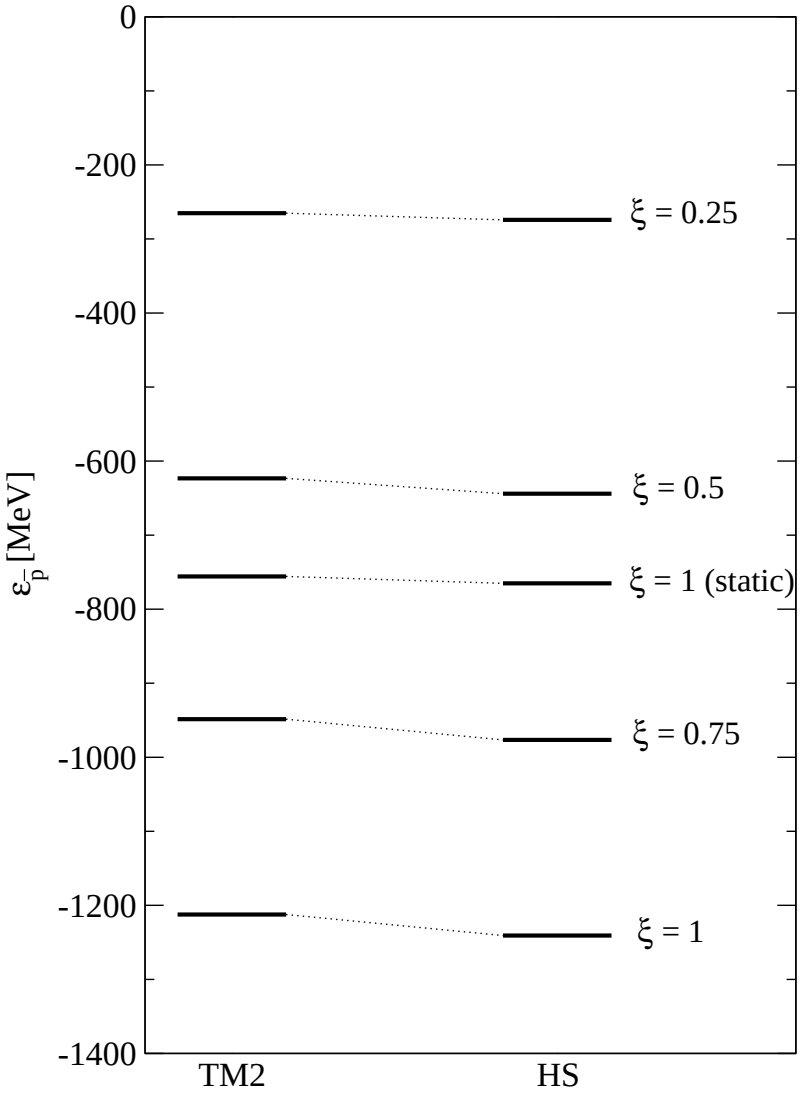

Figure 5.7: The energy levels of the antiproton for different values of the ξ parameter calculated dynamically and the binding energy of the antiproton for $\xi = 1$ in the static approach within both models.

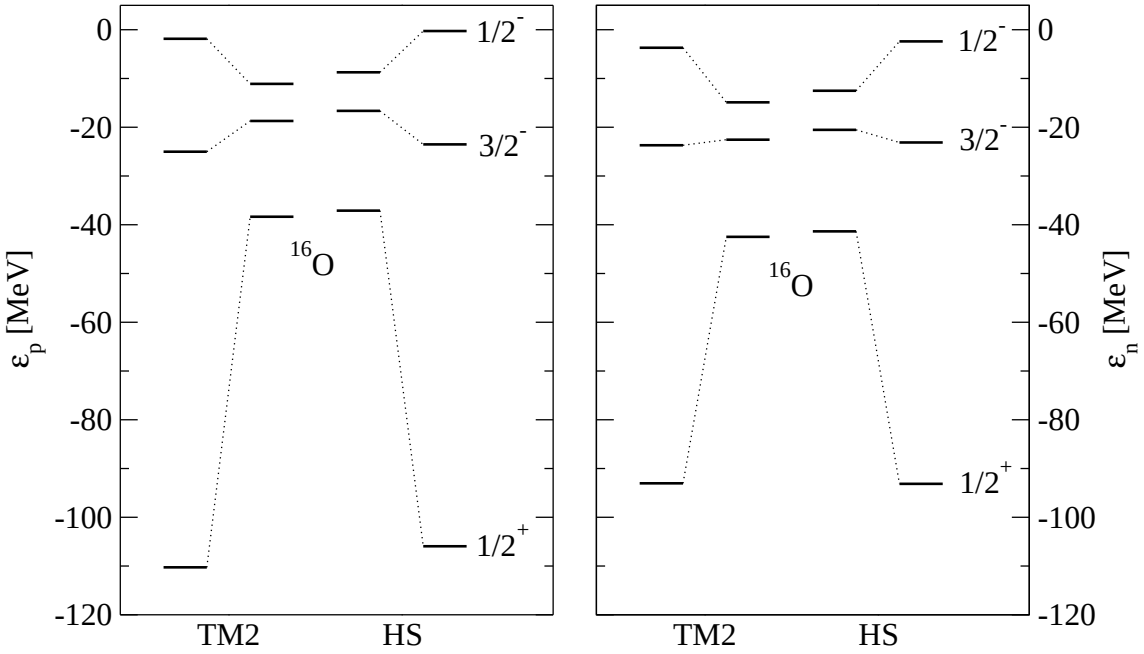

Figure 5.8: The energy levels of protons (left) and neutrons (right) in $^{16}O_{\bar{p}}$ for both parametrization for $\xi = 1$ compared with the energy levels in ^{16}O (in the middle of each figure).

Chapter 6

Discussion and conclusions

In this work the interaction of the antiproton with a nucleus was studied. The goal was to examine the influence of the strongly interacting antiproton on the polarization of a nucleus within the relativistic mean field theory. For this purpose, the ^{16}O nucleus was considered.The coupling constants for the antiproton were obtained using the G-parity transformation of the proton coupling constants. The densities of the core nucleons and their single-particle energies, as well as the densities and single-particle energy of the antiproton inside the nucleus were calculated. Two RMF models were used–the linear model HS and the nonlinear model TM2. Dynamical as well as static calculations were performed in order to illustrate the effect of the polarization of the nuclear core caused by the antiproton.

Large polarization effects on the core nucleons were found. The presence of the antiproton in a nucleus causes compression of the nuclear core. The maximum density in $^{16}\mathrm{O}_{\bar{p}}$ reaches approximately three times the nuclear density in ^{16}O. The extent of the rearrangement of the nucleons depends on the applied parametrization of the RMF model. The models used in this work give different values of nuclear compressibility. The linear model HS gives larger nuclear compressibility than the nonlinear TM2 model. Therefore, the HS model predicts lower central densities of the core nucleons in $^{16}\mathrm{O}_{\bar{p}}$ than TM2. On the other hand, the sizeable changes in the single particle energies of the antiproton as well as nucleons are larger for the HS model because the linear models yield larger meson mean fields than the nonlinear ones. The difference in the total binding energy between ^{16}O and $^{16}\mathrm{O}_{\bar{p}}$ is for the HS model $\triangle B_{HS} = 1157.05$ MeV in absolute value. Within the TM2 model, this difference is lower, $\triangle B_{TM2} = 1131.28$ MeV. To conclude, both models give similar results.

In further studies, it will be desirable to use other sets of parameters for the RMF model which are suitable for the description of nuclear matter at high densities. Such parametrization is, e.g., the FSU-gold parametrization [29] or the model of Kotulič

Bunta and Gmuca [30] which parametrizes the Dirac-Brueckener-Hatree-Fock EOS of asymmetric nuclear matter. These models contain extra cross-coupling term which characterizes the interaction between the ω and ρ mesons.

It is also desirable to perform calculations for other nuclei and to study the dependence of observed effects on the mass number A. We can assume that the polarization of the core nucleons due to the presence of the antiproton will decrease as A increases.

In the present work, the annihilation (absorption) of the antiproton in nuclear matter was not considered. Of course, it must be involved in every realistic model. One should consider a complex potential whose imaginary part describes the absorption of antiproton. The information about the magnitude of the real and imaginary parts of the complex potential can be obtained from experiments with antiprotonic atoms [3, 21, 15]. Another question is the life time of the antiproton in nuclear matter. Whether it is possible that the antiproton exists long enough to cause the compression of nuclear matter. The life time of antiproton inside nuclear matter at normal density is about 2 fm. The estimated life time of deeply bound antiproton inside the dense nuclear matter is about 20 fm [1].

In the further study, we plan to revise the fits of the energy shifts and widths in antiprotonic atoms. This will enable us to determine the value of the parameter ξ for the antiproton coupling constants and the imaginary part of the $\bar{p}$-nucleus potential. Consequently, we will be able to perform more realistic calculations of antiprotonic nuclei.

Appendix A

Notation and conventions

We adhere to the convention of Serot and Walecka [26]. Natural physical units are chosen with $\hbar = c = 1$. Contravariant x_μ and covariant x^μ four vectors are written as

$$x \equiv x^\mu = (t, \vec{x}), \quad x_\mu = (t, -\vec{x}) \tag{A.1}$$

$$\partial^\mu \equiv \frac{\partial}{\partial x_\mu} = \left(\frac{\partial}{\partial t}, -\nabla\right), \quad \partial_\mu \equiv \frac{\partial}{\partial x^\mu} = \left(\frac{\partial}{\partial t}, \nabla\right) \tag{A.2}$$

The Dirac equation for a free particle of mass M reads

$$(i\gamma_\mu \partial^\mu - M)\psi = (i\not{\partial} - M)\psi = 0, \tag{A.3}$$

where we use the Feynman "slash" notation $\not{a} = a_\mu \gamma^\mu$. The gamma matrices $\gamma^\mu = (\gamma^0, \vec{\gamma})$ obey

$$\gamma^\mu \gamma^\nu + \gamma^\nu \gamma^\mu = \{\gamma^\mu, \gamma^\nu\} = 2g^{\mu\nu}, \tag{A.4}$$

where $g^{\mu\nu}$ is a metric tensor given by

$$g^{\mu\nu} = \begin{pmatrix} 1 & 0 & 0 & 0 \\ 0 & -1 & 0 & 0 \\ 0 & 0 & -1 & 0 \\ 0 & 0 & 0 & -1 \end{pmatrix}, \tag{A.5}$$

and in the standard (Dirac-Pauli) realization are given as

$$\gamma^0 = \begin{pmatrix} \mathbb{1} & 0 \\ 0 & \mathbb{1} \end{pmatrix}, \quad \vec{\gamma} = \begin{pmatrix} \vec{\sigma} & 0 \\ 0 & \vec{\sigma} \end{pmatrix}, \tag{A.6}$$

with Pauli matrices defined by

$$\sigma_1 = \begin{pmatrix} 0 & 1 \\ 1 & 0 \end{pmatrix}, \quad \sigma_2 = \begin{pmatrix} 0 & -i \\ i & 0 \end{pmatrix}, \quad \sigma_3 = \begin{pmatrix} 1 & 0 \\ 0 & -1 \end{pmatrix}. \tag{A.7}$$

The nucleon wave functions are considered as isospin doublets, i.e.

$$\psi_i = \begin{pmatrix} \psi_p \\ \psi_n \end{pmatrix}, \tag{A.8}$$

where ψ_p and ψ_n denotes proton and neutron wave functions, respectively.

Bibliography

[1] A.B. Larionov, I.N. Mischustin, L.M Satarov, W. Greiner, Phys. Rev. **C 78** (2008) 014604.

[2] T.J. Bürvenich, W. Greiner, I.N. Mischustin, L.M. Satarov, H. Stöcker, Phys. Rev. **C 71** (2005) 035201.

[3] C.J. Batty, E. Friedman, A. Gal, Phys. Rep. **287** (1997) 385.

[4] J. D. Walecka, Annals of Physics **83** (1974) 491.

[5] B.D. Serot, J.D. Walecka, Int. J. Mod. Phys. E6 (1996) 515.

[6] S. Weinberg, *The quantum theory of fields*, Vol. 1, Cambridge University Press, Cambridge 1995.

[7] D. Griffiths, *Introduction to elementary particles*, John Wiley & Sons, Inc., 1987.

[8] J.Žáček, *Úvod do fyziky elementráních částic*, 1.vydanie, Praha: Karolinum, 2005.

[9] *Particle data group* [online]

URL:<http://pdg.lbl.gov/2010/listings/rpp2010-list-p.pdf>

[cit. 2011-9-3]

[10] G. Gabrielse, X. Fei, K. Helmerson, S.L. Rolstone, R. Tjoelker and T.A. Trainor, Phys. Rev. Lett. **57** (1986) 20.

[11] G.Baur *et al.*, Phys. Lett. **B 368** (1996) 251.

[12] S. Tessaro and OBELIX Collaboration, Nucl. Phys. **A 655** (1999) 230c.

[13] ASACUSA *experiment* [online]

URL:<http://asacusa.web.cern.ch/ASACUSA/home/spsc/phase2-prop.pdf>
[cit. 2011-2-2]

[14] ASACUSA measures antiproton mass with record precision, *Cern Courier* [online], July 2006, [cit 2011-10-3], URL:<http://cerncourier.com/cws/archive/cern/46>

[15] E. Friedman, A. Gal, J. Mareš, Nucl. Phys. **A 761** (2005) 283.

[16] H. Poth, H. Barth, G. Büche, A.D. Hancock, H. Koch, Th. Köhler, A. Kreissl, U. Raich, D. Rohmann, A. Wolf, L. Tauscher, A. Nilsson, M. Suffert, M. Chardalas, S. Dedoussis, H. Daniel, T. von Egidy, F. J. Hartmann, W. Kanert, H.S. Plendl, G. Schmidt, J. J. Reidy, Nucl. Phys. **A 466** (1987) 667.

[17] M. Iwasaki, R. S. Hayno, T. M. Ito, S. N. Nakamura, T. P. Terada, D. R. Gill, L. Lee, A. Olin, M. Salomon, S. Yen, K. Bartlett, G. A. Beer, G. Mason, G. Trayling, H. Outa, T. Taniguchi, Y. Tamashita, R. Seki, Phys. Rev. Lett. **78** (1997) 3067.

[18] G. Beer, A. M. Bragadireanu, M. Cargnelli,. C. Curceanu-Petrascu, J.-P. Egger, H. Fuhrmann, C. Guaraldo, M. Iliescu, T. Ishiwatari, K. Itahashi, M. Iwasaki, P. Kienle, T. Koike, B. Lauss, V. Lucherini, L. Ludhova, J. Marton, F. Mulhauser, T. Ponta, L. A. Schaller, R. Seki, D. L. Sirghi, F. Sirghi, J. Zmeskal, Phys. Rev. Lett. **94** (2005) 212302.

[19] G. Fricke, C. Bernhardt, K. Heilig, L. A. Schaller, L. Schellenberg, E. B. Shera, C. W. De Jager, Atom. Data Nucl. Data Tables 60 (1995) 177.

[20] E. Friedman, A. Gal, Nucl. Phys. **A 724** (2003) 143.

[21] E. Friedman, A. Gal, Phys. Rep. **452** (2007) 89.

[22] P.-G. Reinhardt, Rep. Prog. Phys. **52** (1989) 439.

[23] E. H. Auerbach, C. B. Dover and S. H. Kahana, Phys. Rev. Lett. **46** (1981) 702.

[24] A. J. Baltz, C. B. Dover, M. E. Sainio, A. Gal, G. Tocker, Phys. Rev. **C 32** (1985) 1272.

[25] I.N. Mischustin, L.M. Satarov, H. Stöcker and W. Greiner, Phys. Rev. **C 59** (1999) 3343.

[26] B.D. Serot, J.D. Walecka, *Advances in nuclear physics*. Vol. 16, Plenum Press 1986.

[27] Y. Sugahara, H. Toki, Nucl. Phys. **A 579** (1994) 557.

[28] C.J. Horowitz, B.D. Serot, Nucl. Phys. **A 368** (1981) 503.

[29] B.G. Todd-Rutel, J. Piekarewicz, Phys. Rev. Lett. **95** (2005) 122501.

[30] J. Kotulič Bunta, Š. Gmuca, Phys. Rev. **C 68** (2003) 054318.